Fast Virtual Shadow Projection System as Part of a Virtual Multisensor Assistance System

Dipl.-Ing. Klaus Haskamp [a, d], Dr.-Ing. Dipl.-Phys Markus Kästner [b, d], Prof. Dr.-Ing Eduard Reithmeier[c, d]

[a]Research Associate in the workgroup Production Metrology;
[b]Head of the workgroup Production Metrology;
[c]Head of the Institute of Measurement and Automatic Control;
[d]Institute of Measurement and Automatic Control, Leibniz Universität Hannover, Nienburger Strasse 17, Hannover, Germany

ABSTRACT

The quality test is one of the main components of a production process. The main task of the quality test is the inspection of the relevant geometry parts concerning the predefined tolerance range. To verify, that the relevant geometry parts can be detected with a measurement uncertainty, which is less than the predefined tolerance range, multiple measurements of an appropriate reference specimen have to be done. The related time and money effort is very high and can be reduced using a numerical simulation of the whole measurement process. The measurement uncertainty can be estimated using a virtual measurement process and Monte-Carlo methods. Using the combination of the simulation and Monte-Carlo methods, it is, for example, possible, to calculate the optimal alignment of the workpiece within the measurement volume. Thereby, the optimality criterion can be defined as a minimum of the measurement uncertainty or as a hollistic measurement.

In addition to the estimation of uncertainties, it is possible to use the virtual measurement system as part of an assistance system. The assistance system should provide measurement strategies with respect to different criteria, like the minimisation of the measurement uncertainty. This is the field of research of the subproject B5 of the collaborative research centre 489 (CRC 489), funded by the German Research Foundation (DFG). The main task is the setup of a virtual multisensor assistance system for the calculation of optimised work piece adapted measurement strategies.

In this paper the virtual measurement system and process of a shadow projection system will be explained in detail. Besides the mathematical model, a verification of the simulation and a concept for the estimation of measurement uncertainties will be given.

Keywords: Shadow Projection, Fast Numerical Simulation, Estimation of Measurement Uncertainties, Virtual Measurement System, Virtual Multisensor Assistance System

1. INTRODUCTION

The quality inspection is one of the most important parts of the production process due to the continuous increasing requirements of manufacturing and construction techniques. The main task of the quality inspection is to ensure, that all significant geometry parts can be detected with a measurement uncertainty which is less than the pre-defined work piece tolerances, e.g. the planarity or the cylindricity. A cost and time expensive measurement analysis using an appropriate reference specimen has to be done to estimate the reachable accuracy. The measurement analysis has to be accomplished for each metrological individual case, which enhances the money and time effort, too. Using virtual measurement techniques and Monte-Carlo methods, it is possible to estimate the reachable measurement uncertainty and therewith to reduce the costs, whereas the virtual system is implemented in the computer as a software. The whole calculation is done in the computer and needs only the CAD-model of the work piece. This is a big advantage compared to the usual procedure because the software can

Further author information: (Send correspondence to Klaus Haskamp)
Klaus Haskamp: E-mail: klaus.haskamp@imr.uni-hannover.de, Telephone: +49 (0)511 762 42 84

Modeling Aspects in Optical Metrology III, edited by Bernd Bodermann, Harald Bosse, Richard M. Silver,
Proc. of SPIE Vol. 8083, 80830G · © 2011 SPIE · CCC code: 0277-786X/11/$18 · doi: 10.1117/12.883026

give some feedback and some useful information to the design engineer without the use of a real work piece. For example, the software can tell the design engineer, if the available measurement system can achieve the claimed tolerances.

Another field of application for the virtual measurement systems are virtual multisensor assistance systems. The measurement systems can be integrated in a virtual multisensor assistance system, which is used for the automatic (intelligent) calculation of optimised measurement strategies concerning different criteria.[1,2] For example the criteria can be the minimisation of the measurement time, the holistic measurement or the minimisation of the measurement uncertainty. This is the main field of research of the subproject B5 "Complete Geometry Inspection" of the collaborative research centre 489 (CRC 489) "Process Chain for the Production of Precision Forged High Performance Components", funded by the German Research Foundation (DFG). The main task of the project is the development of a virtual multisensor assistance system, which is build from a fringe projection sensor, a shadow projection sensor, a system of linear axes and a rotation axis. Thereby, the shadow projection system is combined with the rotation axis and a linear axis and the fringe projection sensor is fixed on a system of three linear axes. The assistance system should be used for the calculation of intelligent and work piece specific measurement strategies with respect to the testing of geometric dimensioning and tolerancing. Besides the integration of the named criteria, it is foreseen to determine the best measurement system for the planed measurement task.

Previous research works dealt with the development and the identification of the fringe projection system. This work should be focussed on the numerical simulation of the shadow projection system. Shadow projection systems are applied for contour measurements.[3] Therefore, the measurement object is illuminated from one side with parallel monochromatic laser light. The light is interrupted from the edge of the object and the projected shadow is detected from a CCD row sensor, which is equipped with telecentric projection optics. To calculate the expansion of the projected shadow, the shadow boundaries have to be extracted. Therefore the gray scale values from bright and dark crossings were evaluated using sub pixel methods and interpolated using polynomial functions. The shadow border can be found at the pixel-position, where the interpolated gray scale trend deceeds a predefined digitalisation threshold.

To get a precise simulation model and to have the possibility to simulate the real measurement effects, the theory of wave optics has to be used. The solution of the diffraction integral results in the diffraction images. The modelling of diffraction brings along a high simulation time, especially in the case, that the lenses and the apertures have large dimensions. For the statistical analysis "virtual" multi-measurements have to be executed, which is usually not practical in the case that one single simulation lasts a few hours. Using the virtual shadow projection system for the estimation of measurement uncertainties the simulation time has to be reduced. In this work the numerical efficient simulation of a shadow projection system and a method for the estimation of measurement accuracies will be presented.

At first the virtual measurement system and the used physical fundamentals will be explained in Sec. 2. Special algorithms have been developed and the simulation time can be reduced with nearly the factor $2.7 \cdot 10^3$ to a few seconds for a single simulation. This will be explained in Sec. 2, too. In Sec. 3 the verifications of the virtual simulation model will be given. Sec. 4 deals with the description of the method for the estimation of the measurement uncertainties. In Sec. 5 an example for the analysis of the influence of a system parameter concerning the measurement uncertainties will be shown.

2. VIRTUAL MODEL OF THE SHADOW PROJECTION SYSTEM

In this chapter, the virtual model of the shadow projection system and the used physical fundamentals are explained in detail. Furthermore the simulation procedure is described.

The simulation of the shadow projection system is based on the fundamentals of wave optics. This means, that the integral theorem of Helmholtz and Kirchhoff has to be solved.[4] The integral is written as:

$$U(P_0) = \frac{1}{4 \cdot \pi} \iint_{\Sigma} \left(\frac{\partial U}{\partial \mathbf{n}} \cdot \frac{exp(j \cdot k \cdot r_{01})}{r_{01}} - U \cdot \frac{\partial}{\partial \mathbf{n}} \left(\frac{exp(j \cdot k \cdot r_{01})}{r_{01}} \right) \right) ds, \tag{1}$$

with P_0 as the observation point, $U(P_0)$ as the electric field at the observation point, k as the wave number, r_{01} as the length from the light source to the observation point and $\mathbf{n}$ as the normal vector of the aperture pointing outwards. The integral can be solved using the first Rayleigh-Sommerfeld-solution:

$$U(P_0) = \frac{1}{j \cdot \lambda} \cdot \iint_{\Sigma} A \cdot exp(j \cdot \phi) ds \quad \text{with} \quad A = U(P_1) \cdot \frac{\cos(\mathbf{n}, \mathbf{r_{01}})}{r_{01}} \quad \wedge \quad \phi = k \cdot r_{01}, \tag{2}$$

with λ as the wavelength and $\mathbf{r}_{01}$ as the vector pointing from the aperture to the observation point.

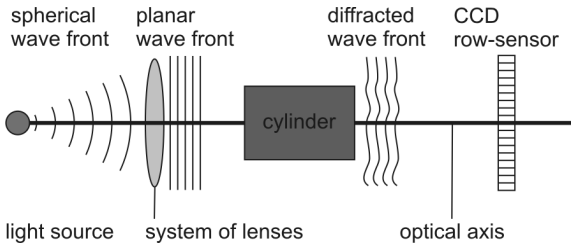

Figure 1. Principle of the used shadow projection system

In Fig. 1 the principle of the used shadow projection system is shown. A point light source sends out a spherical wave front, which is converted into a planar wave front through a system of lenses. Afterwards the planar wave front impignes on the measurement object, which is a cylinder in the figure. The cylinder diffracts the wave front, which is imaged on a CCD-row-sensor.

The used optical componentes are not optimal. To get a precise simulation model, the wave front abberations have to be regarded in the numerical simulation. For this purpose, Zernike polynomial functions can be used for the description of the phase errors $\phi_{Aberr}(x, y)$ and the phase errors were considered as an additional phase term in equation (2):[5]

$$Z_n^m(\rho, \phi) = R_n^m(\rho) \cdot \cos(m \cdot \phi) = \Delta\phi_{Aberr}(x, y) \tag{3}$$

with

$$R_n^m = \sum_{k=0}^{\frac{n-m}{2}} \frac{(-1)^k \cdot (n-k)!}{k! \cdot \left(\left(\frac{n+m}{2}\right) - k\right)! \cdot \left(\left(\frac{n-m}{2}\right) - k\right)!} \cdot \rho^{n-2 \cdot k}, \tag{4}$$

ρ is the normalized radial distance of the point (x, y) and ϕ is the azimuthaly angle. The normalized distance and the azimuthaly angle can be calculated from the coordinates (x, y) of the discrete point. Examples for phase errors are the so called astigmatism or coma, as shown in Fig. 2:[5]

$$Z_{Astig} = \rho^2 \cdot \sin(2 \cdot \theta) \quad \vee \quad Z_{Coma} = \left(3 \cdot \rho^3 - 2 \cdot \rho\right) \cdot \sin(\theta). \tag{5}$$

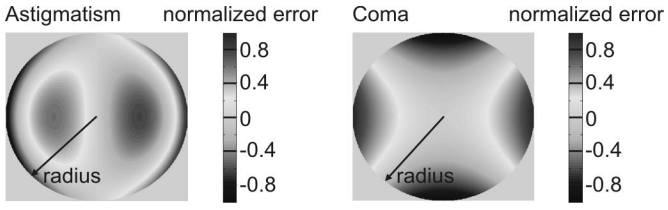

Figure 2. Different wave front aberrations

In the simulation, the electric field is calculated for discrete points, which should be expressed with the post-positioned indices $_{xy}$. Furthermore, the double integral can be converted into a double sum. Using equation (2) and equation (3), the solution of the integral theorem of Helmholtz and Kirchhoff can be written as follows:

$$U_{xy}(P_0) = \frac{1}{j \cdot \lambda} \cdot \sum\sum A \cdot exp(j \cdot \phi) \tag{6}$$

with

$$A = U_{xy}(P_1) \cdot \frac{\cos(\mathbf{n},\mathbf{r_{01}}) \cdot \delta x \cdot \delta y}{r_{01}} \quad \wedge \quad \phi = k \cdot r_{01} + \phi_{Aberr}(x,y). \tag{7}$$

δx and δy are the grid sizes in x- and y-direction.

For the simulation, it is useful to assign a coordinate system to each optical component. In this case, the optical components are the projector lens, the CCD-matrix and the so called reference plane z_0. The use of the reference plane will be described later. Therewith, it is possible, to simulate the misalignment between the optical axis or between the lens and the CCD-matrix. In Fig. 3 the virtual model with the used coordinate systems is shown. Each 3D-point is described with respect to the object coordinate system CS_{Object}. In the real system, as shown in Fig. 1, the CCD is a row sensor. In Fig. 3, the CCD is a CCD-Matrix for the reason of a better visual representation.

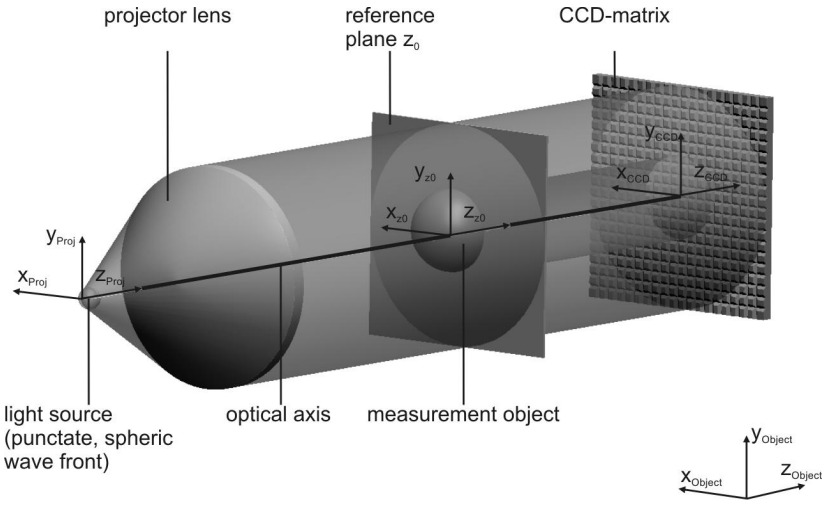

Figure 3. Virtual model with the used coordinate systems

In the following paragraph, the simulation process is explained in detail. The intitialisation part is shown in Fig. 4 and the calculation part is shown in Fig. 6.

At the beginning of the simulation, the system parameters are loaded and the Zernike polynomial functions and the homogen transformation matrices $\mathbf{T}_{hom}$ are initialised. In the next step, the measurement object, in this case a cylinder, is created. The structure of the measurement object is a triangular polygon and is stored in a list L of the form:

$$L = \begin{bmatrix} \mathbf{e}_{11} & \mathbf{e}_{21} & \mathbf{e}_{31} & \mathbf{n}_1 \\ \mathbf{e}_{12} & \mathbf{e}_{22} & \mathbf{e}_{32} & \mathbf{n}_2 \\ \cdots & & & \\ \mathbf{e}_{1i} & \mathbf{e}_{2i} & \mathbf{e}_{3i} & \mathbf{n}_i \\ \cdots & & & \\ \mathbf{e}_{1N} & \mathbf{e}_{2N} & \mathbf{e}_{3N} & \mathbf{n}_N \end{bmatrix}. \tag{8}$$

$\mathbf{e}_{1i}$ to $\mathbf{e}_{3i}$ are the edge points and $\mathbf{n}_i$ is the normal vector of the polygon i, and N is the total number of polygons. The disadvantage of the use of polygons is the restricted accuracy of the replicated surface. Especially

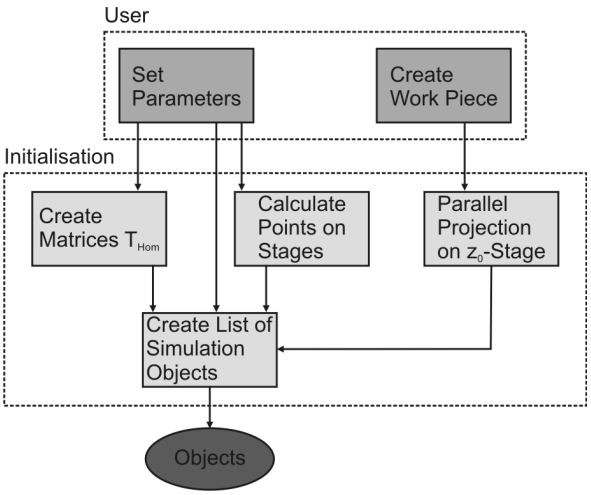

Figure 4. Initialisation schedule of the simulation

the structure of a curved surface is converted into cornered areas. This problem can be reduced through a high number of polygons. Subsequently, the basic simulation is started. During the simulation process, the electric field is calculated for different planar apertures, the so called "stages". The stages are the aperture of the projector lens, the CCD-matrix respectively the CCD row sensor, and the z_0-plane. The z_0-plane is required for the aperture of the measurement object due to the fact, that the Rayleigh-Sommerfeld-solution needed two dimensional apertures.[4] In this case, it is forseen to "measure" 3D-objects, this means, that the 3D-shape has to be transformed into a 2D-aperture. This is done with a central perpective and parallel projection with respect to the xy-axes of the z_0-plane. Then, the aperture of the z_0-plane is build through the points which lie inside the projected and flat body. In the case, that the measurement object is a cylinder, which axis are parallel to the axes of CS_{z0}, the aperture of the z_0-plane is a circular aperture. The verification, that the simplification of the neglecting of the 3D-shape is valid, will be given in Sec. 3.

In the next step, the points of the apertures were calculated. That implies for the z_0-stage, that the points have to be calculated, which lie outside the surface of the projected measurement object, because the electrical field of the points lying inside has no effect concerning the diffraction integral. To get precise simulation results, it is important to have a fine resolution for the discretisation. In the case, that the distance between two points is too big, the phase error between two contiguous points is too big and there are unsolicited aliasing effects. To avoid this problems, the maximum resolution must be estimated. Therefore the principle in Fig. 5 and the following assumption is used:

- ideal lenses $\rightarrow \phi_{Aberr}(x, y) = 0$

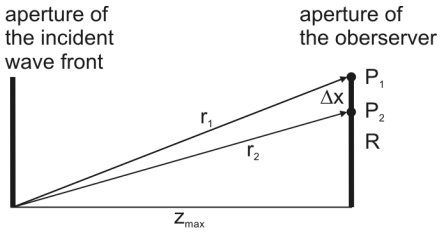

Figure 5. Principle for the estimation of the maximum resolution

To estimate the maximum phase error $\Delta\Phi_{max}$, the phase difference between the points P_1 and P_2 is calculated:

$$\frac{2 \cdot \pi}{\lambda} \cdot (r_1 - r_2) \leq \Delta\Phi_{max}, \tag{9}$$

$$r_1 = \sqrt{R^2 + z_{max}^2}, \tag{10}$$

$$r_2 = \sqrt{(R - \Delta x)^2 + z_{max}^2}, \tag{11}$$

$$\Delta x \leq R - \sqrt{\left(r_1 - \frac{\lambda \cdot \Delta\Phi_{max}}{2 \cdot \pi}\right)^2 - z_{max}^2}, \tag{12}$$

with R as the maximum radius of the aperture, z_{max} as the distance between both apertures and Δx as the maximal resolution. In our case the parameters are nearly:

$$R \approx 5mm, \quad \lambda \approx 653nm, \quad z \approx 80cm. \tag{13}$$

With a maximum allowed phase error $\Delta\Phi_{max} = 45°$ the maximum resolution Δx can be calculated to:

$$\Delta x \approx 13.077\mu m. \tag{14}$$

In Fig. 6, the schedule for the calculation of the intensity on the CCD is shown. At first, the electric field $E_{xy,Proj}$ and the wave front aberrations $\phi_{Aberr,Proj}(x, y)$ on the projector lens are calculated. This information is used in combination with the projected work piece to compute $E_{xy,z0}$. In the last step, $E_{xy,CCD}$ respectively $I_{xy,CCD}$ is computed. The intensity on the CCD can be used for further analysis, e.g. the estimation of the shadow boundaries with the aid of subpixel methods.

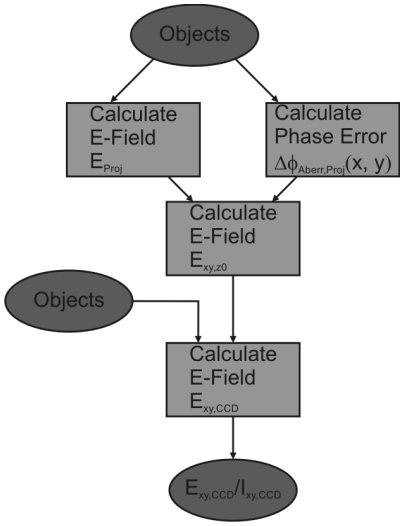

Figure 6. Schedule of the calculation of the intensity on the CCD

Due to the fact, that the execution of one simulation lasts nearly 10 hours, it is necessary for the Monte-Carlo-simulations to accelerate the execution time. Therefore, a special algorithm was developed, which should be shortly discussed. The algorithm is based on the interpolation of diffraction images. Therefore, two different resolutions were required. The first resolution is called the start resolution δx_{start} and δy_{start}, is used for the discretisation of the observation aperture and is set to a high value of $100\mu m$. For this reason, the number of points, for which the double sum has to be executed, are reduced and the simulation decreases. The second

resolution is called the interpolation resolution δx_{int} and δy_{int} and is set to a value $< 10\mu m$. The electrical field respectively the amplitude A and the phase ϕ of the incident wave front, which is available only for a mesh with a grid size of δx_{start} and δy_{start}, is interpolated down to δx_{int} and δy_{int}. Thereby, the number of points, for which the integral theorem of Helmholtz and Kirchhof has to be solved, can be reduced coincidently with a low resolution.

3. VERIFICATION

In this chapter, the verifications of the virtual simulation model are given. To verify, that the treatment of the 3D-bodies as 2D-apertures is valid, the diffraction images of cylinders with different length are compared with the diffraction image of a sphere. Thereby, the cylinders and the sphere have all the same radius. The test objects are shown in Fig. 7. The test objects are illuminated from one side with parallel monochromatic red laser light with a wavelength of $\lambda \approx 653nm$. The shadow is imaged using a camera from the "AVT-PIKE-series" with $2048x2048$ pixel and a pixel size of $7.4\mu m\,(H)\,x7.4\mu m\,(V)$.

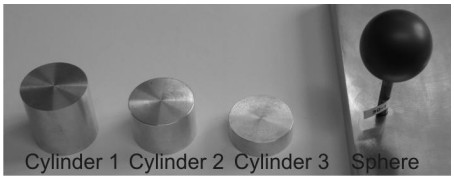

Figure 7. Test objects for the verification

The different diffraction images are shown in Fig. 8. The image points out, that the diffraction images look similar. For a quantitative analysis, the pattern of cylinder 3 and the sphere were compared. Therefore the images were lied on top of each other using correlation techniques. The result is also shown in Fig. 8. The comparison points out, that the maximum error is less than 5%. This means, that the simplification is valid.

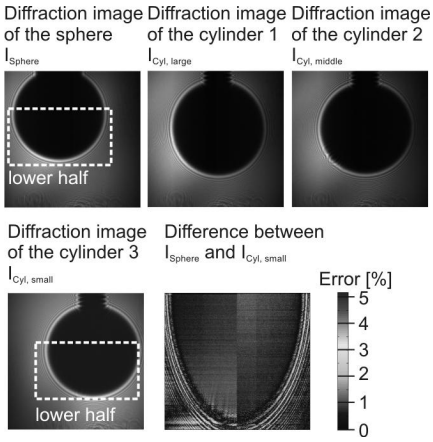

Figure 8. Diffraction images of the cylinders and the sphere

4. METHOD FOR THE ESTIMATION OF MEASUREMENT UNCERTAINTIES

In this chapter, the method for the estimation of measurement uncertainties is explained in detail. Based on the virtual model and the simulation procedure, described in Sec. 2, the diffraction pattern was calculated for a fix work piece alignment and a set of parameters. In the following, the real target value, the edge position, is determined using subpixel methods. The principal is shown in Fig. 9. The noisy "measurement" signal f_1 is interpolated with the function f_2. The interpolated edge e_{int} can be found at the position, where f_2 deceeds

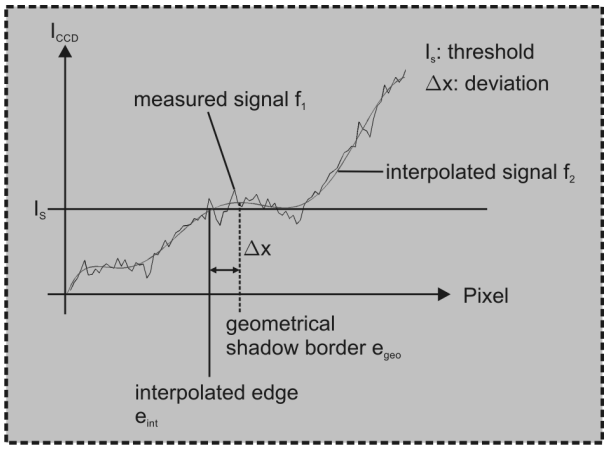

Figure 9. Interpolation of the intensity on the CCD

respectively exceeds a pre-defined threshold I_s. e_{int} differs from the geometrical edge position e_{geo} due to the fact, that the signal f_1 is noisy and the CCD-matrix/row-sensor has a finite pixel size.

In Fig. 10 the procedure for the estimation of measurement uncertainties is shown. The measurement uncertainty is the uncertainty of the interpolated edge positions and can be estimated with the standard deviation of all simulated edge positions. At first the work piece is created and the system parameters are set, see Sec. 2. In the following, the diffraction image of the CCD and the analysis of the edge position for one single simulation is executed and e_{int} is saved. Previous to the next simulation, the system parameters are varied on the basis of appropriate propability density functions. Therewith, it is possible, to emulate the variance of the CCD-intensity and the edge positions. The execution of the simulations is closed in the case, that the number of simulations N_{Sim} is large enough ($N_{Sim} > 100$). After that, the standard deviation and the mean value of all e_{int} are calculated.

5. ANALYSIS OF INFLUENCE FACTORS CONCERNING THE MEASUREMENT UNCERTAINTY USING THE EXAMPLE OF CRANK SHAFTS

In this chapter, the measurement uncertainty of the edge positions of the upper main bearing of a two cylinder crank shaft is analysed with respect to an intrinsic system parameter. This parameter is the wave front aberration of the projector lens.

To analyse the influence of the intrinsic system parameters with respect to the measurement uncertainty, only the intrinsic parameters are varied during the Monte-Carlo-simulation. Here, the so called Coma of the projector lens is used for the wave front aberrations and the maximum phase error $\phi_{Coma,max}$ at the boundary of the aperture (at radius R) is the strayed value.

In Fig. 11 the correlation between increasing coma and the estimated measurement uncertainty of the right edge is shown. The figure points out a linear trend between the phase error and the estimated uncertainty of the detected edge positions.

6. CONCLUSION

In this paper the virtual model of a shadow projection system is described in detail. The used physical fundamentals are explained and a verification of the virtual model is given. In the following, the procedure for the estimation of measurement uncertainties and an example for the analysis of a system parameter with respect to the measurment uncertainty is given.

The virtual system can be integrated in an assistance system, whereas the assistance system is build up from different measurement systems. The assistance system should estimate, which measurement system is the best system for the measurement task. The decision can be made with respect to different criteria, like the minimisation of the measurement uncertainty or the minimisation of the measurement time.

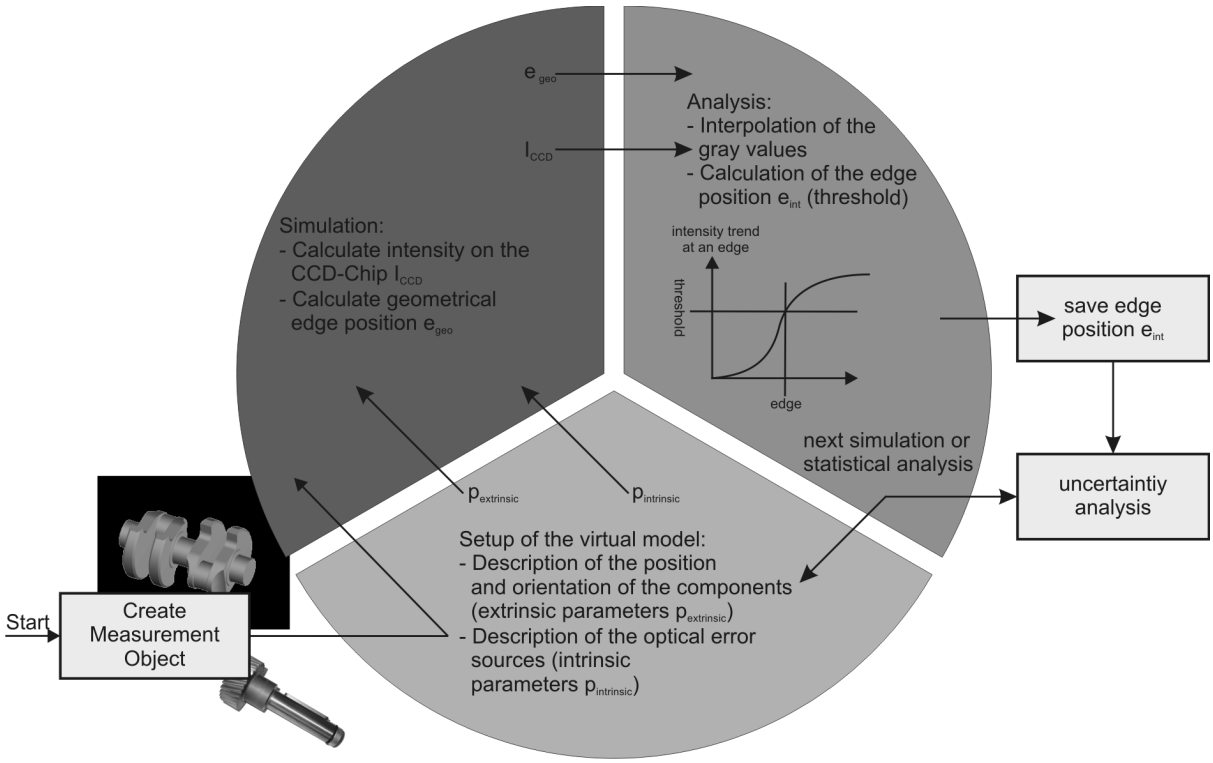

Figure 10. Procedure for the estimation of measurement uncertainties

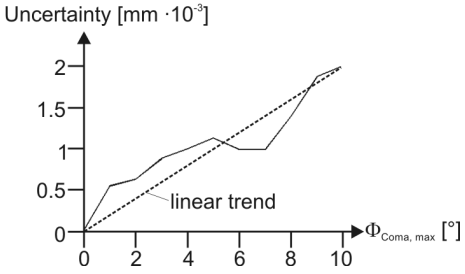

Figure 11. Correlation between Coma and measurement uncertainty

REFERENCES

[1] Weckenmann, A., Hartmann, W. and Weickmann, J., "Model and simulation of fringe projection measurements as part of an assistance system for multi-component fringe projection sensors", Proceedings of SPIE Vol. 7102 (2008)

[2] Weckenmann, A., Hartmann, W. and Weickmann, J., "Multi-component fringe projection sensors: Assistance system for short and robust inspection processes", Proceedings 2008 NCSL International Workshop and Symposium (2008)

[3] Kästner, M., [Optische Geometrieprüfung präzisionsgeschmiedeter Hochleistungsbauteile], Dissertation, Leibniz Universität Hannover (2008)

[4] Goodman, J., [Introduction to Fourier Optics], Roberts & Company Publishers, (2005)

[5] Singer, W., Totzeck, M. and Gross, H., [Handbook of Optical Systems], Wiley-VCH Verlag GmbH & Co. KGaA, (2005)

ACKNOWLEDGMENTS

The authors wish to acknowledge teh German Research Foundation (DFG) for the financial support of the Subproject B5 of the collaborative research centre 489.